Joint Inversion of Electromagnetic and Seismic Data Based on Structural Constraints Using Variational Born Iteration Method

Tian Lan, Hai Liu, *Member, IEEE*, Na Liu, Jinghe Li, Feng Han, and Qing Huo Liu, *Fellow, IEEE*

***Abstract*— An efficient 2-D joint full-waveform inversion method for electromagnetic and seismic data in a layered medium background is developed. The joint inversion method based on the integral equation (IE) method is first proposed in this paper. In forward computation, the IE method is employed, which usually has smaller discretized computation domain and less cumulative error compared with the finite-difference method. In addition, fast Fourier transform is used to accelerate the convolution between Green's functions and induced sources due to the shift invariance property of the layered Green's functions in the horizontal direction. In the inversion model, the cross-gradient function is incorporated into the cost function of the separate inversion to enforce the structure similarity between electric conductivity and seismic-wave velocity. We use the improved variational Born iteration method and two different iteration strategies to minimize the cost function and reconstruct the contrasts. Several typical models in geophysical applications are used to validate our joint inversion method, and the numerical simulation results show that joint inversion can improve the inversion results when compared with those from the separate inversion.**

***Index Terms*— Stabilized biconjugate gradient fast Fourier transform (BCGS-FFT), joint inversion, structure constraints, variational Born iteration method (VBIM).**

I. Introduction

ELECTROMAGNETIC (EM) and seismic data are widely used in geophysical exploration. For a long term, their inversion processes were performed individually. These two modalities have their own advantages and disadvantages. Seismic inversion cannot provide information to distinguish oil from water. The EM data inversion is sensitive to conductivity variations, but it usually has lower resolution than the seismic inversion, since the low-frequency EM field for geophysical application in lossy ground is a diffusive field [1], [2]. In addition, the conductivity difference between oil and gas is negligible, which leads them to be indistinguishable by EM inversion. Fortunately, this can be compensated by seismic inversion. Therefore, joint inversion of EM and seismic data can avoid their own disadvantages but combine their advantages, and thus improve the capabilities of geophysical evaluation [3].

The concept of joint multiphysical inversion was first proposed in [4], and acquired great development in the past decades. Two main approaches are suggested for joint inversion. One is based on the petrophysics of the rocks [5]–[7], and the other is to make use the structure similarity [8]–[12]. In the first method, the relationship between seismic data and EM data is established through petrophysical links [7], such as Archie's equations [13] and Waxman and Smits' equation [14]. In the second method, the structural constraint function is added to the original cost function to enforce the structure similarity [9], [11], [15], [16]. Compared with the second method, a stronger constraint is used in the first method, which usually leads to more accurate results. However, the equations of petrophysical relationships are usually problem-dependent. Therefore, the first inversion method can be applied only to limited situations. Fortunately, the second inversion method is not subject to specific problems, and therefore, it can easily be extended to various data.

Joint inversion based on the structural constraint function is usually performed by combining separate inversion methods in different physical areas. One typical joint inversion method is to use full-waveform inversion (FWI) for all physical fields [11]. In the joint FWI model, the finite-difference (FD) is often used for forward computation, and the adjoint approach is often used to calculate the Fréchet derivative matrix for inverse computation [11], [16]–[19]. In this paper, we use the integral equation (IE) method to perform the forward computation. The IE method has a smaller computational domain and accumulated error than the FD method [20]. When the forward calculations are realized with the IE method, we often solve inverse problems with the Born iteration method (BIM) [21], the distorted BIM [22], the variational BIM (VBIM) [23], or the contrast source inversion [24]. VBIM was first proposed for the conductivity reconstruction in an axisymmetric medium for induction well-logging application, which shows a fast and stable convergence in the inversion iteration [23], [25]. We use the improved VBIM in the inversion computation, since the Fréchet derivative matrix can be obtained with just once

Manuscript received March 30, 2017; revised July 17, 2017; accepted August 28, 2017. Date of publication September 22, 2017; date of current version December 27, 2017. This work was supported by the National Natural Science Foundation of China under Grant 41390453, Grant 11501481, and Grant 41504120. *(Corresponding authors: Feng Han; Qing Huo Liu.)*

T. Lan, H. Liu, N. Liu, and F. Han are with the Institute of Electromagnetics and Acoustics, Department of Electronic Science, Xiamen University, Xiamen 361005, China (e-mail: feng.han@xmu.edu.cn).

J. Li is with the College of Earth Science, Guilin University of Technology, Guilin 530001, China.

Q. H. Liu is with the Department of Electrical and Computer Engineering, Duke University, Durham, NC 27708 USA (e-mail: qhliu@duke.edu).

Color versions of one or more of the figures in this paper are available online at http://ieeexplore.ieee.org.

Digital Object Identifier 10.1109/TGRS.2017.2749240

integration in VBIM, which is easier and faster than the adjoint approach. Moreover, due to the IE method, the direct inversion parameters in VBIM are the contrasts, which are the relative physical parameters without units. Therefore, we no longer consider the different dimensions and units of the ultimate inversion parameters that are often considered in other joint inversion methods [11], [26], [27].

In this paper, we apply the joint inversion of electrical conductivity and seismic velocity through enforcing the structure similarity constraints and performing the VBIM algorithm. Detailed descriptions of the forward model, separate models, and the joint inversion model are given. Then, we test both the separate inversion models and the joint inversion model using two groups of synthetic measured data, and compare the accuracy and efficiency of these models. The antinoise ability of the joint inversion model is also evaluated.

II. Methods

A. Forward Model

In the 2-D model, the computational domain is defined in the xz plane and there is no variation in the y-direction. In geophysical applications, the z-axis is usually downward and represents the depth, while the x-axis stands for the horizontal distance.

For EM modeling, we restrict to the 2-D transverse magnetic case. This means that the electric line source is infinitely long in the y-direction, and the electric field exists only in the y-direction. Then the equation of the electric field in Maxwell's equations is reduced to a scalar Helmholtz equation

$$\left(\Delta + k_{\mathrm{EM}}^2\right) E_y = j\omega_{\mathrm{EM}}\mu_0 J_y \tag{1}$$

where $k_{\mathrm{EM}}^2 = \omega_{\mathrm{EM}}^2\mu_0(\epsilon - j\sigma/\omega_{\mathrm{EM}})$ represents the complex wave number of the EM field.

For seismic modeling, we use scalar acoustic approximation, which is better posed in inverse problems [28]. On the assumption that the mass density is constant, the acoustic equations are simplified into the Helmholtz equation [29]

$$\left(\Delta + k_S^2\right) p = -f \tag{2}$$

where $k_S = \omega_S/c$, c is the acoustic velocity and f denotes the volume source distribution.

In the forward model, it is assumed that the electric and acoustic parameters of the scatters that are buried in layered media are known and field values at the receivers are to be solved. For the volume IE method, the total field is split into the incident field and the scattered field. The incident field is the field when the scatters are not present in the layered media. Since (1) and (2) have similar mathematical expressions, the IE can be expressed as

$$\phi^{\mathrm{tot}}(\mathbf{r}) = \phi^{\mathrm{inc}}(\mathbf{r}) + k_i^2 \int_s g(\mathbf{r}, \mathbf{r}') \cdot \chi(\mathbf{r}')\phi^{\mathrm{tot}}(\mathbf{r}')d\mathbf{r}' \tag{3}$$

where k_i is the wavenumber of EM or acoustic in the ith layer, and $\chi = (k^2 - k_i^2)/k_i^2$ is contrast. ϕ is the field that can denote E_y or p. The superscripts tot and inc mean the total field and the incident field, respectively. g is 2-D Green's function in the layered media that has the same expression for (1) and (2). 2-D Green's function in homogeneous media has the form of the second kind Hankel's function. Its semiclosed form in layered media can be solved by the wave decomposition method or the transmission line analogy method. Both the methods have been proved feasible for 3-D layered Green's functions [30], [31]. Equation (3) cannot be solved analytically. The method of moment is always used to solve it numerically in a discretized system. However, the direct matrix solver is time-consuming. In this paper, we use the pulse basis functions and the stabilized biconjugate gradient (BCGS) iteration method to solve the total field in (3). Moreover, the fast Fourier transform (FFT) is applied to accelerate the convolution between Green's functions and induced sources, because the layered Green's function is shift invariant in the horizontal direction [3].

B. Separate Inversion

In the inversion model, it is assumed that the fields at the receivers are known and the contrast χ is to be solved. In order to solve them iteratively, we first use the Born approximation at each iteration in the IE, i.e., the total field is approximated by the incident field [23], [25]. This approximation is reasonable only for weak scattered fields. For most geophysical exploration using EM waves, the scattered fields are weak, because the wavelength and the skin depth are much larger than the scatterer size, and the attenuation caused by the background medium also plays a role. However, for the seismic-wave exploration, it depends on the frequency and the scatterer size. Numerical experiments show that Born approximation can be employed when the misfit between the incident field and the total field is less than 30%. In this paper, we do not test geophysical exploration cases having strong scattering, so Born approximation is feasible. In this way, the scattered field can be expressed as

$$\phi^{\mathrm{sct}}(\mathbf{r}) = k_i^2 \int_s g(\mathbf{r}, \mathbf{r}') \cdot \chi(\mathbf{r}')\phi^{\mathrm{inc}}(\mathbf{r}')d\mathbf{r}' \tag{4}$$

where χ is the direct inversion parameter. We can get the variational representation of ϕ^{sct} about χ

$$\delta\phi^{\mathrm{sct}}(\mathbf{r}) = k_i^2 \int_s g(\mathbf{r}, \mathbf{r}') \cdot \delta\chi\ (\mathbf{r}')\phi^{\mathrm{inc}}(\mathbf{r}')d\mathbf{r}' \tag{5}$$

where $\delta\phi^{\mathrm{sct}}$ means the misfit between the computed scattered field and the measured scattered field. Meanwhile, $\delta\chi$ means the misfit between the reconstructed contrast and the real contrast in the computational domain. In this way, the problem is linearized in the discretized IE, which is expressed as

$$\delta\phi^{\mathrm{sct}} = [L]\delta\chi \tag{6}$$

where $[L]$ is a matrix. Each element of $[L]$ can be expressed as

$$L_{mn} = k_i^2 \int_s g\left(\mathbf{r}_m, \mathbf{r}_n'\right) \cdot \phi^{\mathrm{inc}}\left(\mathbf{r}_n'\right)d\mathbf{r}' \tag{7}$$

where m is the global index of the receiver and n is the global index of the discretized grid in the inversion domain. It should be noted that L keeps unchanged during the whole inversion process due to the Born approximation, so we compute the integration just once. In the strong scattering case, L should be computed through total field precisely and updated in each iteration. Unlike the VBIM algorithm given in [23],

we improve the VBIM with normalization to balance the contribution of each term in (8). The cost function with the regularization term in the qth iteration step is defined as

$$F(\delta\chi_q) = \frac{\left\|\delta\phi_{q-1}^{\text{sct}} - [L]\delta\chi_q\right\|^2}{\left\|\delta\phi_{q-1}^{\text{sct}}\right\|^2} + \gamma^2 \frac{\|\delta\chi_q\|^2}{\|\delta\chi_{q-1}\|^2} \tag{8}$$

where $\delta\phi_{q-1}^{\text{sct}}$ represents the field misfit computed in the $q-1$th iteration and γ^2 is the regularization parameter. This linear least square problem is equivalent to solve

$$([L]^\dagger[L] + \frac{\gamma^2\left\|\delta\phi_{q-1}^{\text{sct}}\right\|^2}{\left\|\delta\chi_{q-1}\right\|^2}\mathbf{I})\delta\chi_q = [L]^\dagger\delta\phi_{q-1}^{\text{sct}} \tag{9}$$

with the conjugate gradient (CG) method [32], where † denotes complex conjugate and transpose.

C. Joint Inversion

The separate inversion algorithm discussed in Section II-B is performed for the electric and pressure fields, independently. Joint inversion is to combine the EM and acoustic information together. The key point is using the structure similarity to enforce the gradients of electric and acoustic contrasts aligned along the same line. The idea is to minimize the cross-gradient function, which is given by [9]

$$\mathbf{t}(x,z) = \nabla\chi^{\text{EM}}(x,z) \times \nabla\chi^{S}(x,z) \tag{10}$$

where "×" is the outer product. Since the contrasts are relative values without units, there is no need to balance the contribution of different physical parameters, which is used in available structure constraints joint inversion [9], [11], [27], [33], [34]. Different from the forward difference to expand [9, eq. (10)], we utilize the central difference to gain the second-order accuracy [33]

$$t_{i,j} = \left(\frac{\chi_{i,j+1}^{\text{EM}} - \chi_{i,j-1}^{\text{EM}}}{2\Delta z}\right)\left(\frac{\chi_{i+1,j}^{S} - \chi_{i-1,j}^{S}}{2\Delta x}\right) - \left(\frac{\chi_{i+1,j}^{\text{EM}} - \chi_{i-1,j}^{\text{EM}}}{2\Delta x}\right)\left(\frac{\chi_{i,j+1}^{S} - \chi_{i,j-1}^{S}}{2\Delta z}\right) \tag{11}$$

where i and j denote the indexes of the discretized grids in the x-direction and the z-direction, respectively. There are two methods to construct the joint cost function. One is to combine both the cost functions of the EM and acoustic separate inversions into a unified cost function as

$$\begin{aligned} F\left(\delta\chi_q^{\text{EM}}, \delta\chi_q^{S}\right) &= \frac{\left\|\delta\phi_{q-1}^{\text{EM,sct}} - [L^{\text{EM}}]\delta\chi_q^{\text{EM}}\right\|^2}{\left\|\delta\phi_{q-1}^{\text{EM,sct}}\right\|^2} \\ &\quad + \gamma^2\frac{\left\|\delta\chi_q^{\text{EM}}\right\|^2}{\left\|\delta\chi_{q-1}^{\text{EM}}\right\|^2} + \frac{\left\|\delta\phi_{q-1}^{S,\text{sct}} - [L^{S}]\delta\chi_q^{S}\right\|^2}{\left\|\delta\phi_{q-1}^{S,\text{sct}}\right\|^2} \\ &\quad + \gamma^2\frac{\left\|\delta\chi_q^{S}\right\|^2}{\left\|\delta\chi_{q-1}^{S}\right\|^2} + w^2\frac{\left\|\mathbf{t}\left(\chi_q^{\text{EM}}, \chi_q^{S}\right)\right\|^2}{\left\|\mathbf{t}\left(\chi_{q-1}^{\text{EM}}, \chi_{q-1}^{S}\right)\right\|^2}. \end{aligned} \tag{12}$$

Minimization of the cost function in (12) as a whole often leads to an ill-posed problem as mentioned in [11]. Therefore, we do not use this method in this paper. Instead, we use the second method. The cost functions, including the terms of the cross-gradient function, are defined. When the cross-gradient function is added to the cost function used in the separate inversion, the cost function in joint inversion is obtained as

$$\begin{aligned} F(\delta\chi_q^{\phi}) &= \frac{\left\|\delta\phi_{q-1}^{\phi,\text{sct}} - [L^{\phi}]\delta\chi_q^{\phi}\right\|^2}{\left\|\delta\phi_{q-1}^{\phi,\text{sct}}\right\|^2} \\ &\quad + \gamma^2\frac{\left\|\delta\chi_q^{\phi}\right\|^2}{\left\|\delta\chi_{q-1}^{\phi}\right\|^2} + w^2\frac{\left\|\mathbf{t}\left(\chi_q^{\phi}, \chi^{\text{other}}\right)\right\|^2}{\left\|\mathbf{t}\left(\chi_{q-1}^{\phi}, \chi^{\text{other}}\right)\right\|^2} \end{aligned} \tag{13}$$

where w^2 denotes the weighting factor and ϕ can express EM or seismic. There are two strategies to minimize the cost function in (13).

Strategy-1 is that the EM inversion and seismic inversion are executed alternately. The flowchart of this strategy is shown in Fig. 1. The cross-gradient function in one physical inversion is based on the latest parameters that are acquired in the last iteration performed in the other physical inversion, and thus the EM inversion and seismic inversion are executed, alternately.

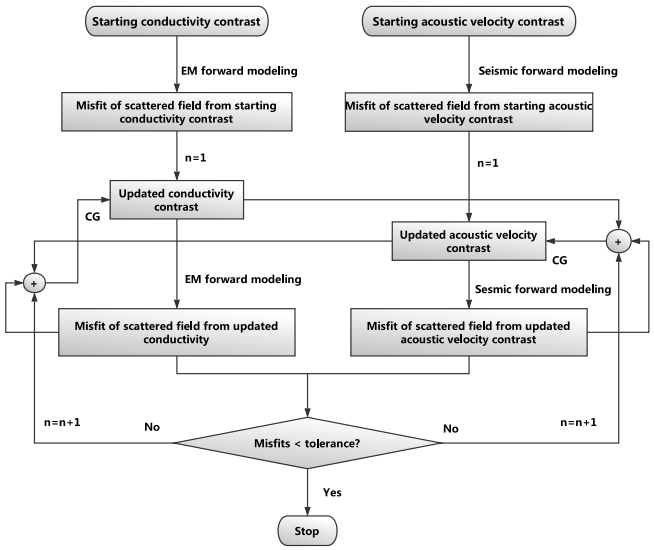

Fig. 1. Flowchart of joint inversion with alternate iterations.

Strategy-2 is that the cross-gradient function in one physical inversion is based on the final result of the other physical inversion. Since the resolution of seismic inversion is usually better than that of EM inversion in geophysical application [2], we can first retrieve the seismic parameters with (8). Then, EM inversion is performed in (13) with the seismic parameters fixed in the cross-gradient function. Once the EM parameter is acquired, we substitute it into (13) and fix it, and then solve the acoustic contrast iteratively.

To realize the linearization of the cross-gradient function $\mathbf{t}$, we approximate it in the present iteration with the first-order Taylor series expansion around its value in the previous iteration [9]

$$\mathbf{t}(\chi_q) \cong \mathbf{t}(\chi_{q-1}) + [B]\delta\chi_q \tag{14}$$

where $[B]$ is the Jacobi matrix of $\mathbf{t}$ about χ and $\delta\chi_q = \chi_q - \chi_{q-1}$. Note that (13) is similar to (8) except that the term of

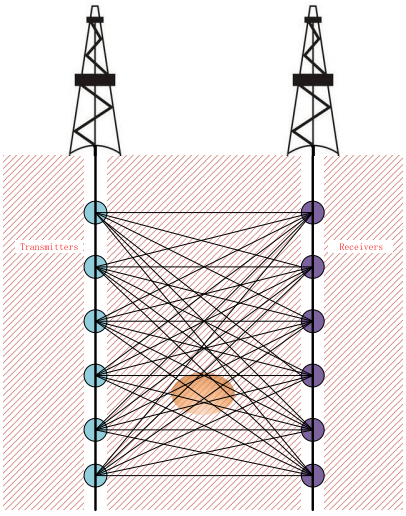

Fig. 2. Cross-well scenario. Transmitters and receivers are placed in the two wells. The domain of interest is located between the two wells.

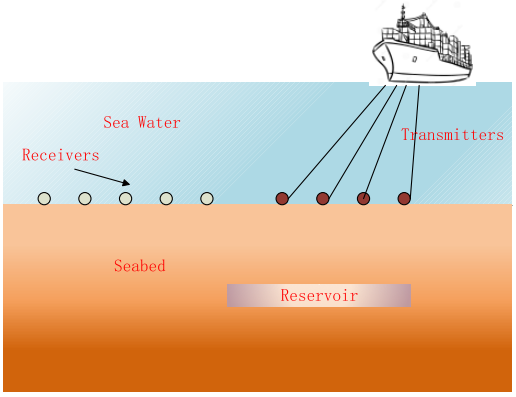

Fig. 3. Layered ocean scenario. Transmitters and receivers are placed near the seafloor. Our goal is to find the reservoirs below the seafloor.

cross-gradient is added. In order to employ the CG method to find $\delta\chi_q$ to minimize F, we transform (13) to [35]

$$([L]^\dagger[L] + \frac{\gamma^2\left\|\delta\phi^{\text{sct}}_{q-1}\right\|^2}{\|\delta\chi_{q-1}\|^2}\mathbf{I} + \frac{w^2\left\|\delta\phi^{\text{sct}}_{q-1}\right\|^2}{\|\mathbf{t}_{q-1}\|^2}[B]^\dagger[B])\delta\chi_q = [L]^\dagger\delta\phi^{\text{sct}}_{q-1} - [B]^\dagger\mathbf{t}_{q-1}. \quad (15)$$

This equation can be directly solved by the CG iteration method [36]. Besides the maximum iteration numbers and minimum field data misfit be directly solved by the CG iteration, the iteration process is also terminated when the inversion parameters are almost unchanged in two successive iterations.

III. Numerical Assessment

To verify our joint inversion algorithm, we use two typical geophysical models, the cross-well model, and the layered ocean model, which are widely used in geophysical applications. Their scenarios are shown in Figs. 2 and 3, respectively.

A. Cross-Well Model

As shown in Fig. 4, the true model has a homogeneous background with an electrical conductivity of 0.5 S/m and an acoustic velocity of 2500 m/s. The inversion domain size

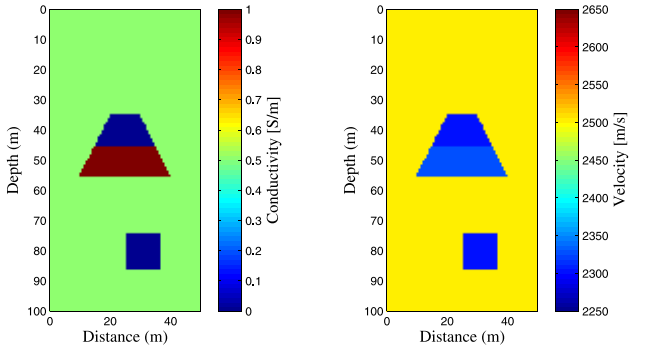

Fig. 4. True cross-well model. (a) Conductivity distribution. (b) Acoustic velocity distribution. Transmitters distribute uniformly from depth = 0 m to depth = 100 m with an interval of 5 m in the vertical line at distance = −1 m and distance = 51 m, respectively. Receivers distribute vertically with 1-m offset of transmitters.

is 50 m × 100 m. There are two regions buried in the reservoir. The top structure is a trapezoid that contains oil in the upper layer and water in the next layer. The bottom structure is a rectangular box filled with oil. The oil has an electrical conductivity of 0.001 S/m and an acoustic velocity of 2300 m/s. The water has an electrical conductivity of 1.0 S/m and an acoustic velocity of 2330 m/s. The contrast of acoustic velocities between oil and water is very small, and thus the interface is hard to be discerned.

We test our joint inversion algorithm using just a pair of frequencies: 500 Hz for EM measurements and 150 Hz for seismic measurements. The transmitters and receivers are arranged to be staggered. There are 21 transmitters distributed uniformly between depth = 0 m and depth = 100 m in the vertical line at distance = −1 m and distance = 51 m, respectively. And there are 21 receivers distributed uniformly between depth = 2.5 m and depth = 102.5 m in the vertical line at distance = −1 m and distance = 51 m, respectively. Thus, the total number of data sets for EM and acoustic measurements is 1764 × 2. The measured data used in the inversion are generated by our forward solver based on the BCGS-FFT algorithm, which are validated by comparing them with COMSOL simulations. In the inversion, we assume that the background parameters are known as *a priori*, since several numerical experiments show that the retrieved conductivity or velocity are closely related to the background parameters. The inversion domain is discretized into 75 × 150 cells with the cell size of 0.67 m × 0.67 m. Thus, the total number of EM and seismic inversion parameters is 11 250 × 2. In our inversion process, the factors γ and w in (13) are always set as 0.1 and 0.3 separately, which are efficient choices validated by numerical tests. For the initial model, we use a homogeneous medium with $\chi_1 = 0.01$ and $\delta\chi_0 = 0.01$ to avoid the denominator of the second term in (13) to be zero.

The inversion results are shown in Fig. 5. From Fig. 5(d), we find that the seismic inversion by VBIM can reconstruct the profile well including the acoustic velocity and the shapes. But it is far enough to distinguish the oil zone from the water zone using seismic inversion alone. As is shown in Fig. 5(a),

TABLE I
MISFITS FOR DIFFERENT INVERSION METHODS IN CROSS-WELL MODEL WHEN NOISE-FREE

Inversion type	Field misfit(%)		Model misfit(%)		Cross-gradients
	Electric field	Pressure	Conductivity	Velocity	
Separate inversion	3.616	0.525	23.756	0.797	4.771×10^{-2}
Joint inversion of strategy 1	1.418	0.987	26.794	0.787	2.067×10^{-4}
Joint inversion of strategy 2	2.556	0.248	31.341	0.778	2.364×10^{-4}

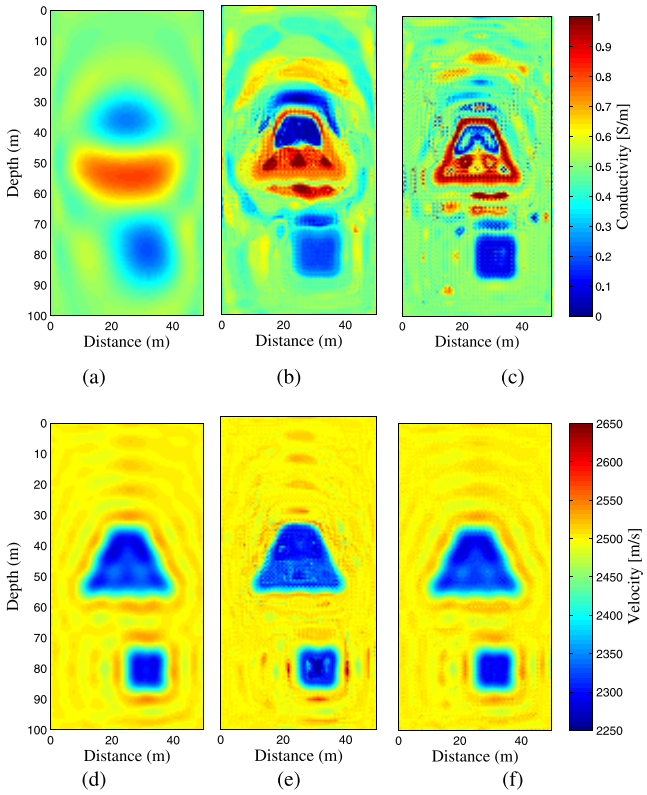

Fig. 5. Inversion results for the cross-well model when noise-free. Reconstructed profile of conductivity in (a) separate inversion, (b) joint inversion with strategy-1, and (c) joint inversion with strategy-2. Reconstructed profile of acoustic velocity in (d) separate inversion, (e) joint inversion with strategy-1, and (f) joint inversion with strategy-2.

EM inversion result reflects the contrast of conductivities well, which helps us to differentiate oil from water directly. However, EM inversion has a poor resolution, which leads to the unclear structure shapes. Fortunately, this can be improved by joint inversion. As shown in Fig. 5(b) and (c), the low resolution of EM inversion results can be compensated with the nice structure information provided by seismic inversion. It should be noted that several clutters show up in the joint inversion images. However, they have no interference to our judgments for the reservoir underground. The acoustic parameters from joint inversion also show some improvements. As shown in Fig. 5(e), the reconstructed profiles of the velocity using the joint inversion strategy-1 become closer to the real model, since the interface between the oil and the water is inverted directly.

The data misfits for inversion processes are shown in Fig. 6. Because the iterations terminate when the data misfit is smaller than a prescribed threshold or keeps almost unchanged,

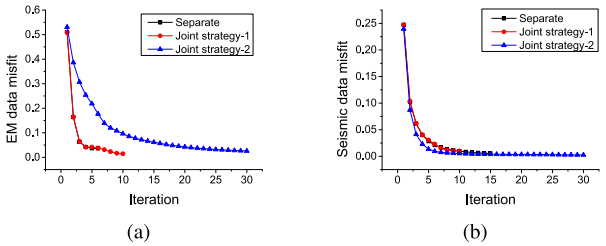

Fig. 6. Inversion convergence process in the cross-well model. (a) EM data misfits. (b) Seismic data misfits.

the iteration numbers are different for the separate or different joint strategies. We can see that the inversion processes are stable without oscillation. The iteration of separate or joint inversion with strategy-1 converges faster than that of joint inversion with strategy-2 for the EM data. However, for seismic data inversion, the convergence speeds have no big difference for three methods. This actually reflects the clutters in the reconstructed results. The appearance of the clutters means that the inversion iteration tries several times instead of converging smoothly to the true values. As shown in Fig. 5(c), the clutters are severe, so the joint inversion with strategy-2 for the EM data is slow.

Both the field and model misfits when iterations terminated for this case are summarized in Table I. Through joint inversion, the norm of the cross-gradient function reduces by two orders of magnitude. This means that the structure difference in the reconstructed electric conductivity and acoustic velocity profiles becomes smaller. The data misfit of EM is reduced in joint inversion compared with separate inversion. And the model misfits of the acoustic velocity also decrease. However, the model misfits of conductivities become larger. This is caused by those clutters outside the original scattering objects, which are shown in Fig. 5(b) and (c). In this cross-well model, the average time of one iteration step is 45 s for EM inversion and 23 s for seismic inversion in an Intel i5-6500 CPU with a memory of 8 GB.

Then, we consider the data contaminated with random noise. The joint inversion results for the signal-to-noise ratio (SNR) $=$ 6 dB are shown in Fig. 7. The location of buried objects is still obvious although the structures have some degree of deformation. In addition, it is obvious that the inversion by seismic waves has stronger antinoise ability. From the data misfits and model misfits given in Table II, we can see that joint inversion also improves the seismic inversion results although the misfit absolute values are larger than those without noise. In order to evaluate the antinoise ability of our joint inversion algorithm, we plot the iteration-terminated data misfits and model misfits versus different SNR values in Fig. 8. In general, the misfits decrease as the SNR

TABLE II
MISFITS FOR DIFFERENT INVERSION METHODS IN CROSS-WELL MODEL WHEN SNR = 6 dB

Inversion type	Field misfit(%)		Model misfit(%)		Cross-gradients
	Electric field	Pressure	Conductivity	Velocity	
Separate inversion	6.249	9.871	26.417	1.152	2.306×10^{-1}
Joint inversion of strategy 1	6.719	10.036	25.294	1.072	3.407×10^{-2}
Joint inversion of strategy 2	7.363	9.807	31.093	0.917	8.786×10^{-4}

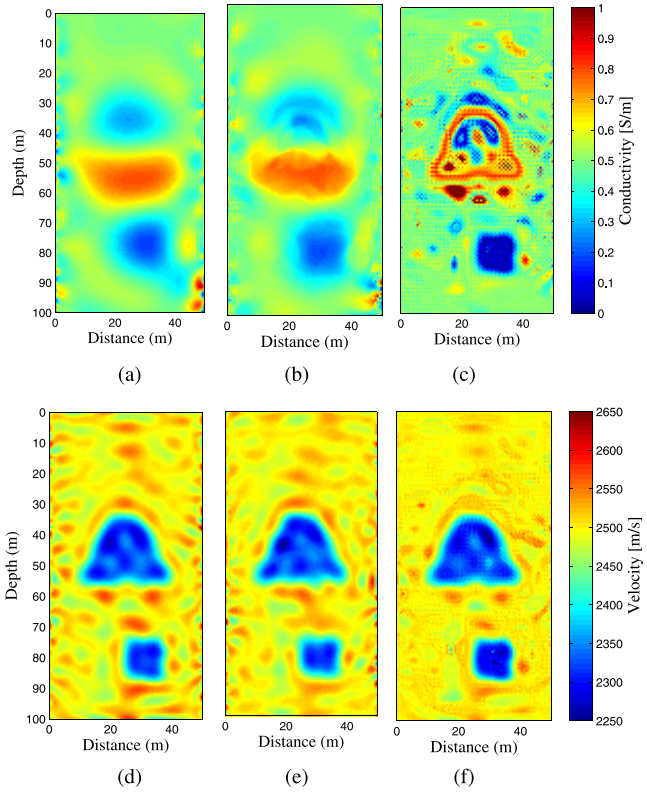

Fig. 7. Inversion results for the cross-well model when SNR = 6 dB. Reconstructed profile of conductivity in (a) separate inversion, (b) joint inversion with strategy-1, and (c) joint inversion with strategy-2. Reconstructed profile of acoustic velocity in (d) separate inversion, (e) joint inversion with strategy-1, and (f) joint inversion with strategy-2.

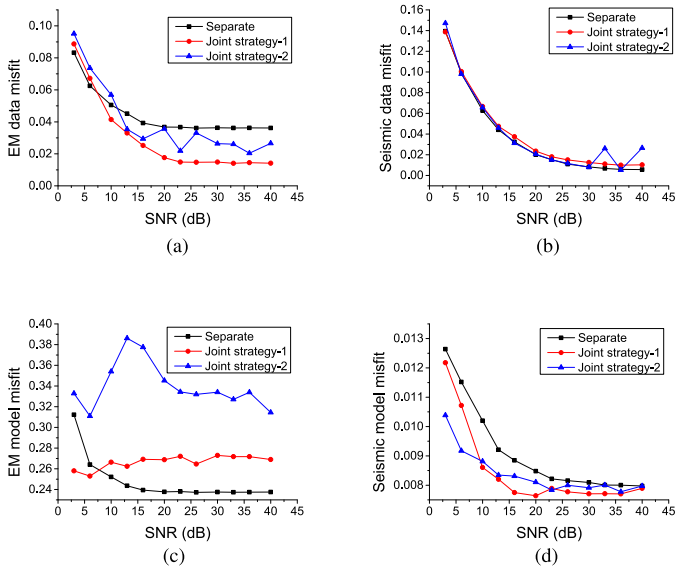

Fig. 8. Data misfits and model misfits change with the SNR in the cross-well model. Data misfits of (a) EM and (b) seismic waves. Model misfits of (c) EM and (d) seismic waves.

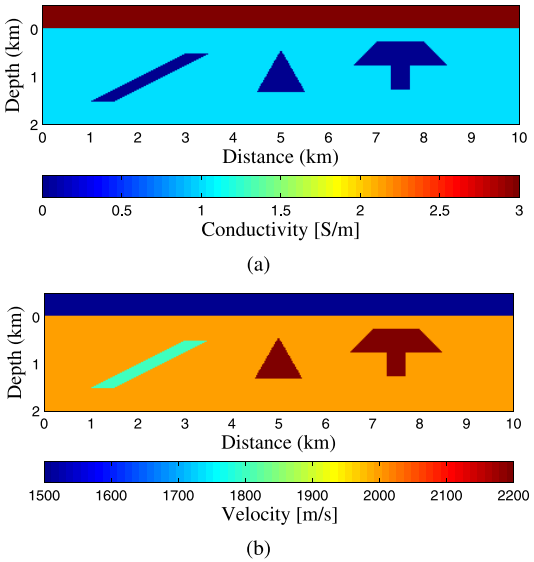

Fig. 9. True half-space approximate ocean model. (a) Conductivity distribution. (b) Acoustic velocity distribution. Transmitters distribute uniformly from distance = −1 km to distance = 11 km with an interval of 200 m at depth = −50 m. Receivers distribute horizontally with −100 m offset of transmitters.

increases. But, due to the random noises, the misfits can fluctuate in some points. Comparing Fig. 8(c) and (d), we can see that the antinoise ability by seismic waves is better than that by EM waves. Not only model misfits are smaller but also they decrease more stably as the SNR increases for seismic waves.

B. Approximate Ocean Model

In the second example, we imitate the ocean, including both the sea water and the seabed, as is shown in Fig. 9. The upper space is the seawater, whose conductivity is 3 S/m and acoustic velocity is 1500 m/s. The lower space is the seabed with a conductivity of 1 S/m and an acoustic velocity of 2000 m/s. In this model, we utilize Green's function in layered media to reduce the computation domain. There are also three different structures buried in the seabed. They all have a conductivity of 0.001 S/m, which can be oil or gas. The left structure is a slope with an acoustic velocity of 1800 m/s, which can denote the gas reservoir. The middle structure is a triangle with an acoustic velocity of 2200 m/s. The right structure shows a small rectangle hidden under a big trapezoid, whose acoustic velocity is 2200 m/s. The middle and right structures can denote the oil reservoirs.

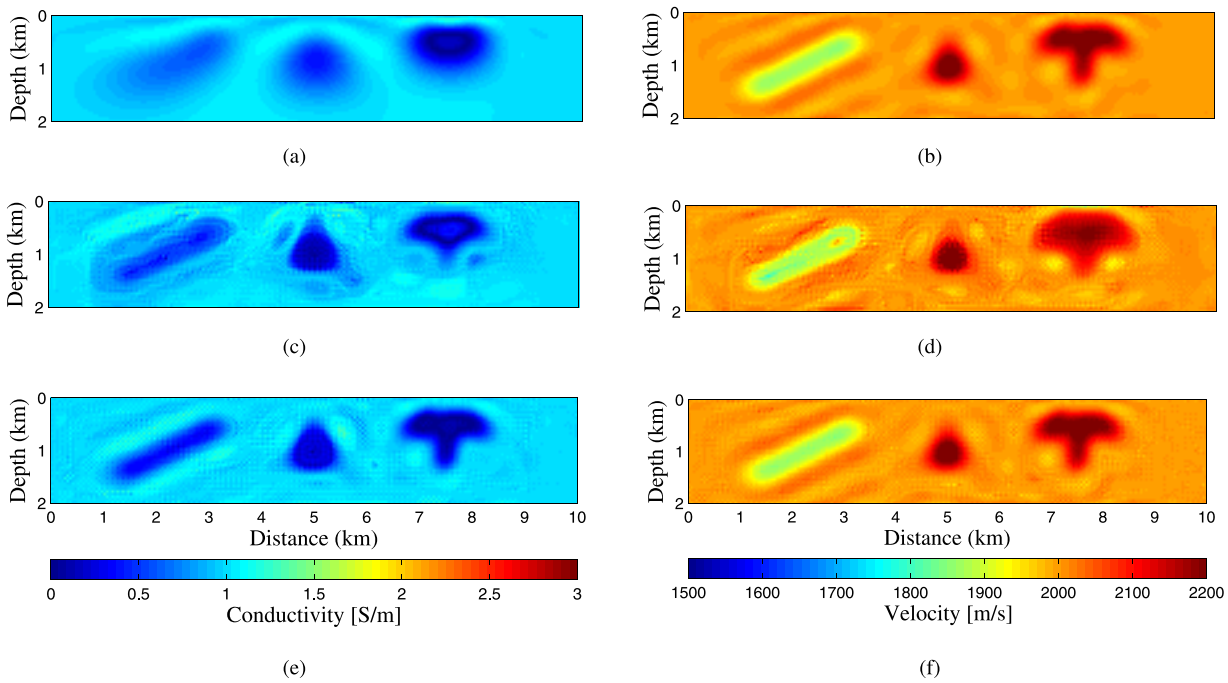

Fig. 10. Inversion results for the approximate ocean model when noise-free. Reconstructed profile of (a) conductivity and (b) acoustic velocity in the separate inversion. Reconstructed profile of (c) conductivity and (d) acoustic velocity in the joint inversion with strategy-1. Reconstructed profile of (e) conductivity and (f) acoustic velocity in the joint inversion with strategy-2.

TABLE III
MISFITS FOR DIFFERENT INVERSION METHODS IN APPROXIMATE OCEAN MODEL WHEN NOISE-FREE

Inversion type	Field misfit(%)		Model misfit(%)		Cross-gradients
	Electric field	Pressure	Conductivity	Velocity	
Separate inversion	0.297	0.586	21.144	1.548	9.421×10^{-6}
Joint inversion of strategy 1	4.870	6.515	19.141	1.869	2.564×10^{-8}
Joint inversion of strategy 2	0.249	0.796	16.382	1.556	2.185×10^{-8}

We place 61 transmitters equally from distance $= -1$ km to distance $= 11$ km at the horizontal line of depth $= -50$ m. And the receivers locate between distance $= -1.1$ km and distance $= 10.9$ km at the depth $= -50$ m. The controlled-source EM source frequency is 0.25 Hz. The seismic source frequency is 1.2 Hz. The computational domain is 10 km $\times$ 2 km. We discretize the domain into 200×40 cells, and the cell size is 50 m $\times$ 50 m. The parameters γ and ω used are the same as in the cross-well model.

First, we invert the data without noise. The inversion results are shown in Fig. 10. We can see that the acoustic velocity profiles by separate inversion shown in Fig. 10(b) are well reconstructed, while the conductivity profiles shown in Fig. 10(a) are blurry. However, when we employ joint inversion and add the structural constraints, the conductivity profiles become more discernible, as is shown in Fig. 10(c) and (e). There is no big difference for the convergence rates in both separate and joint inversions, as is shown in Fig. 11. The average time of one inversion iteration is 11 s for EM inversion and 13 s for seismic inversion. We also evaluate the misfits and list the results in Table III. Unlike in the cross-well model, there are only a few weak clutters in the reconstructed results for this approximate ocean model. Therefore, the model misfit of conductivity is reduced

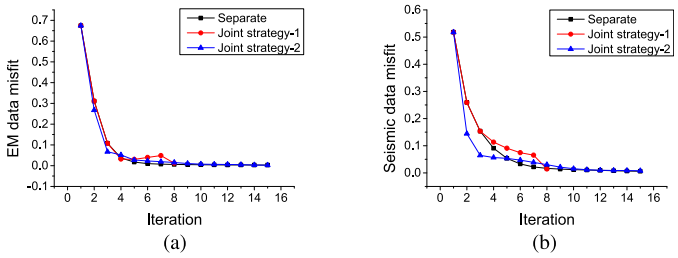

Fig. 11. Inversion convergence process in the approximate ocean model. (a) EM data misfit. (b) Seismic data misfit.

obviously by joint inversion through two strategies. The joint inversion with strategy-2 shows better performance in this model than that with strategy-1. Moreover, joint inversion lowers the norm of cross-gradient function by two orders of magnitude. It should be noted that the acoustic velocity from joint inversion by strategy-1 is even worse than that of separate inversion, as is listed in Table III and shown in Fig. 10(b) and (d). This is probably due to the fact that the low resolution of EM inversion can sometimes compromise the retrieved acoustic velocity in joint inversion, although it helps to discern the interface between the oil and the water in the previous example.

TABLE IV
MISFITS FOR DIFFERENT INVERSION METHODS IN APPROXIMATE OCEAN MODEL WHEN SNR = 6 dB

Inversion type	Field misfit(%)		Model misfit(%)		Cross-gradients
	Electric field	Pressure	Conductivity	Velocity	
Separate inversion	8.186	9.883	25.348	1.664	3.268×10^{-5}
Joint inversion of strategy 1	8.037	10.630	21.719	1.732	5.300×10^{-8}
Joint inversion of strategy 2	8.901	11.394	19.186	1.642	5.328×10^{-8}

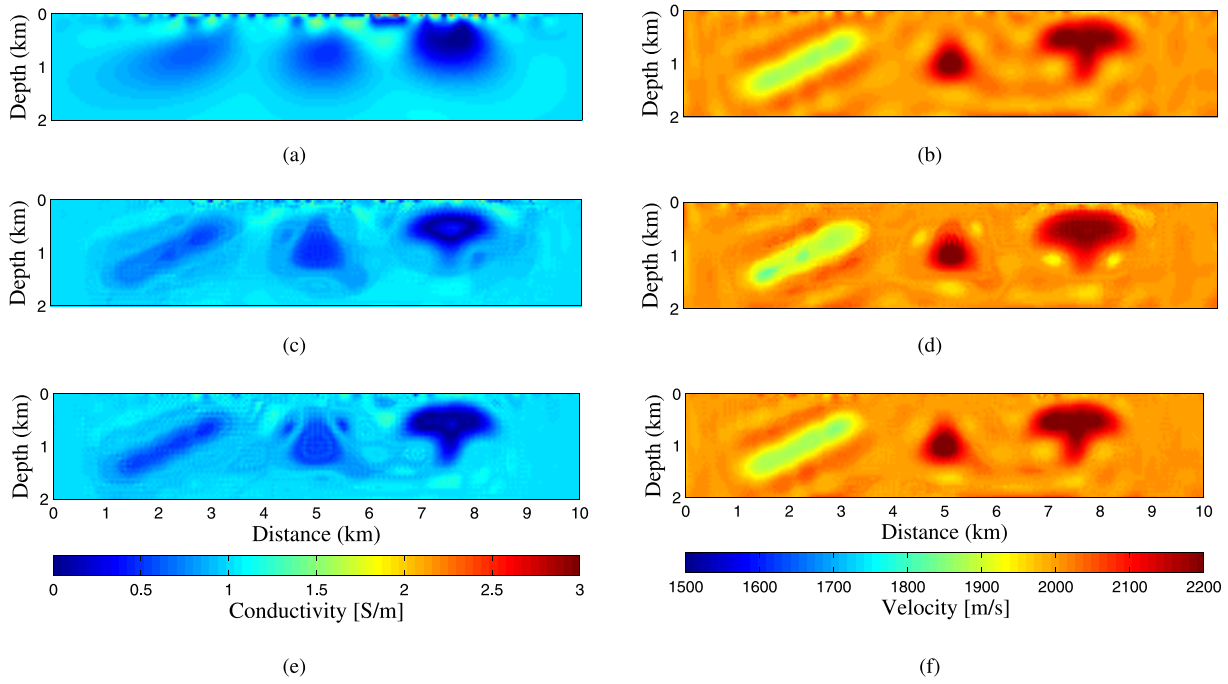

Fig. 12. Inversion results for the approximate ocean model when SNR = 6 dB. Reconstructed profile of (a) conductivity and (b) acoustic velocity in the separate inversion. Reconstructed profile of (c) conductivity and (d) acoustic velocity in the joint inversion with strategy-1. Reconstructed profile of (e) conductivity and (f) acoustic velocity in the joint inversion with strategy-2.

Similar to the cross-well model, we also invert the scattered field data with noise. The inversion results for SNR = 6 dB are shown in Fig. 12. The data misfits and model misfits are listed in Table IV. The reconstructed acoustic velocity profile in Fig. 12(b) is also appreciable. But the reconstructed conductivity profile in Fig. 12(a) is obviously worse than that shown in Fig. 10(a). Through joint inversion, the reconstructed conductivity profile shown in Fig. 12(c) and (e) is enhanced. And their model misfits are reduced. We further show the model misfits and the data misfits versus SNR in Fig. 13. Similar to the cross-well model, the inversion by seismic waves has better antinoise ability. We note that the model misfit of acoustic velocity from joint inversion by strategy-1 seems becoming larger with the increase in SNR, as is shown in Fig. 13(d). The possible reason is as follows. We try to reconstruct the objects through minimizing the data misfit and the cross gradient in the cost function. Comparing Figs. 10(c) and 12(c), we find that the clutters are more prominent when the SNR is larger, i.e., when the noise is weaker. When inversion iterations try to match the structure similarity, clutters will show up in the reconstructed acoustic velocity profiles [shown in Fig. 10(d)], and they will finally increase the model misfits. While for the reconstructed conductivity profiles by joint inversion, the main structures are inverted better than those clutters [shown in Fig. 10(c)], and thus the model misfits become smaller.

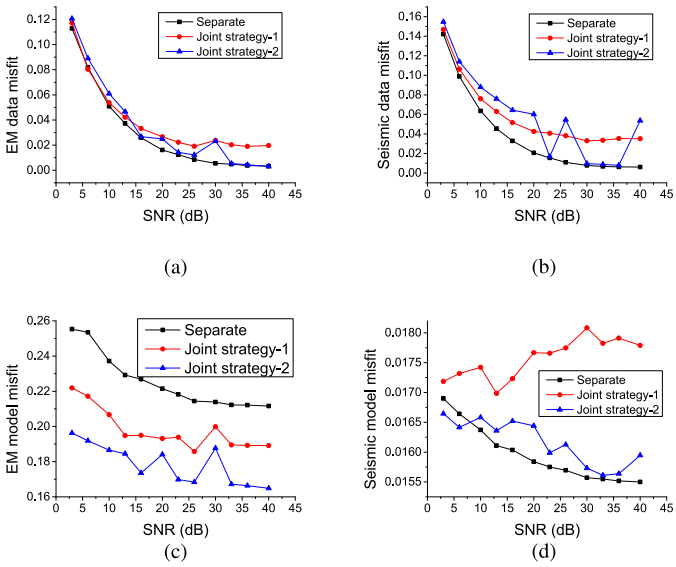

Fig. 13. Data misfits and model misfits change with the SNR in the approximate ocean model. Data misfits of (a) EM and (b) seismic waves. Model misfits of (c) EM and (d) seismic waves.

IV. Conclusion

In this paper, we develop a joint inversion method based on the structure similarity between electric conductivity and acoustic velocity. This model can be applied to a variety of geophysical inversions without the consideration of the dimension of different physical parameters. In the forward computation, the IE is adapted to avoid the large computational domain and to reduce the accumulated error. The EM and acoustic total fields are solved by the BCGS-FFT method where FFT is applied to accelerate the operation between Green's functions and induced sources. In the inversion model, the improved VBIM is used to obtain smoother and fast convergent results. During all the forward and inverse iterations, Green's functions are computed only once.

We tested our joint inversion algorithm with two strategies using the cross-well model and the approximate ocean model. The simulated results of both the cases show that joint inversion can compensate the own disadvantages of separate inversions. In the separate EM inversion, the shapes of the reconstructed conductivity profiles are unclear although the conductivity values are correct. At the same time, the separate seismic inversion cannot distinguish oil from water directly as the EM inversion. This is improved by enforcing the conformity between conductivity and velocity profiles through introducing the cross-gradient function in the joint inversion model. Both the model misfit and cross-gradient function values are reduced through joint inversion. In addition, the antinoise experiments show that the reconstructed profiles approach the true models even with SNR $=$ 6 dB. Therefore, our joint inversion method not only can give reliable results but also has a certain antinoise ability. Moreover, it is not difficult to include more physical parameters in our joint model, since the forward computation for each physical parameter is performed individually and the inversion iteration can be executed alternately.

References

[1] P. Harris and L. MacGregor, "Determination of reservoir properties from the integration of CSEM and seismic data," *First Break*, vol. 24, pp. 15–21, Nov. 2006.

[2] S. Constable, "Ten years of marine CSEM for hydrocarbon exploration," *Geophysics*, vol. 75, no. 5, pp. 75A67–75A81, 2010.

[3] L.-P. Song, E. Şimşek, and Q. H. Liu, "A fast 2D volume integral-equation solver for scattering from inhomogeneous objects in layered media," *Microw. Opt. Technol. Lett.*, vol. 47, no. 2, pp. 128–134, 2005.

[4] K. Vozoff and D. L. B. Jupp, "Joint inversion of geophysical data," *Geophys. J. Int.*, vol. 42, no. 3, pp. 977–991, 1975. [Online]. Available: http://gji.oxfordjournals.org/content/42/3/977.short

[5] G. M. Hoversten *et al.*, "Direct reservoir parameter estimation using joint inversion of marine seismic AVA and CSEM data," *Geophysics*, vol. 71, no. 3, pp. C1–C13, 2006.

[6] P. Dell'Aversana, G. Bernasconi, F. Miotti, and D. Rovetta, "Joint inversion of rock properties from sonic, resistivity and density well-log measurements," *Geophys. Prospecting*, vol. 59, no. 6, pp. 1144–1154, Nov. 2011.

[7] G. Gao, A. Abubakar, and T. M. Habashy, "Joint petrophysical inversion of electromagnetic and full-waveform seismic data," *Geophysics*, vol. 77, no. 3, pp. WA3–WA18, 2012.

[8] M. A. Meju, L. A. Gallardo, and A. K. Mohamed, "Evidence for correlation of electrical resistivity and seismic velocity in heterogeneous near-surface materials," *Geophys. Res. Lett.*, vol. 30, no. 7, p. 1373, 2003.

[9] L. A. Gallardo and M. A. Meju, "Joint two-dimensional DC resistivity and seismic travel time inversion with cross-gradients constraints," *J. Geophys. Res. Solid Earth*, vol. 109, p. B03311, 2004.

[10] L. A. Gallardo, "Multiple cross-gradient joint inversion for geospectral imaging," *Geophys. Res. Lett.*, vol. 34, p. L19301, 2007.

[11] W. Hu, A. Abubakar, and T. M. Habashy, "Joint electromagnetic and seismic inversion using structural constraints," *Geophysics*, vol. 74, no. 6, pp. R99–R109, 2009.

[12] M. Moorkamp, A. W. Roberts, M. Jegen, B. Heincke, and R. W. Hobbs, "Verification of velocity-resistivity relationships derived from structural joint inversion with borehole data," *Geophys. Res. Lett.*, vol. 40, no. 14, pp. 3596–3601, 2013.

[13] G. E. Archie, "The electrical resistivity log as an aid in determining some reservoir characteristics," *Trans. AIME*, vol. 146, no. 1, pp. 54–62, 1942.

[14] M. H. Waxman and L. J. M. Smits, "Electrical conductivities in oil-bearing shaly sands," *Soc. Petroleum Eng. J.*, vol. 8, no. 2, pp. 107–122, 1968.

[15] A. Tryggvason and N. Linde, "Local earthquake (LE) tomography with joint inversion for P- and S-wave velocities using structural constraints," *Geophys. Res. Lett.*, vol. 33, p. L07303, 2006.

[16] L. A. Gallardo and M. A. Meju, "Structure-coupled multiphysics imaging in geophysical sciences," *Rev. Geophys.*, vol. 49, p. 2010RG000330, 2011.

[17] R. G. Pratt, C. Shin, and G. J. Hick, "Gauss–Newton and full Newton methods in frequency–space seismic waveform inversion," *Geophys. J. Int.*, vol. 133, no. 2, pp. 341–362, 1998.

[18] M. Moorkamp, B. Heincke, M. Jegen, A. W. Roberts, and R. W. Hobbs, "A framework for 3-D joint inversion of MT, gravity and seismic refraction data," *Geophys. J. Int.*, vol. 184, no. 1, pp. 477–493, 2011.

[19] A. Abubakar, G. Gao, T. M. Habashy, and J. Liu, "Joint inversion approaches for geophysical electromagnetic and elastic full-waveform data," *Inverse Problems*, vol. 28, no. 5, p. 55016, 2012.

[20] W. Chew *et al.*, *Integral Equation Methods for Electromagnetic and Elastic Waves*. San Rafael, CA, USA: Morgan & Claypool, 2008.

[21] Y. M. Wang and W. C. Chew, "An iterative solution of the two-dimensional electromagnetic inverse scattering problem," *Int. J. Imag. Syst. Technol.*, vol. 1, no. 1, pp. 100–108, 1989.

[22] W. C. Chew and Y. M. Wang, "Reconstruction of two-dimensional permittivity distribution using the distorted Born iterative method," *IEEE Trans. Med. Imag.*, vol. 9, no. 2, pp. 218–225, Jun. 1990.

[23] N. Zaiping, Y. Feng, Z. Yanwen, and Z. Yerong, "Variational Born iteration method and its applications to hybrid inversion," *IEEE Trans. Geosci. Remote Sens.*, vol. 38, no. 4, pp. 1709–1715, Jul. 2000.

[24] P. M. van den Berg, A. L. van Broekhoven, and A. Abubakar, "Extended contrast source inversion," *Inverse Problems*, vol. 15, no. 5, pp. 1325–1344, 1999.

[25] Y. Zhang, R. Wang, and Y.-T. Chen, "Stability of rapid finite-fault inversion for the 2014 M_w6.1 South Napa earthquake," *Geophys. Res. Lett.*, vol. 42, no. 23, pp. 10263–10272, 2015.

[26] L. A. Gallardo and M. A. Meju, "Characterization of heterogeneous near-surface materials by joint 2D inversion of dc resistivity and seismic data," *Geophys. Res. Lett.*, vol. 30, no. 13, p. 1658, 2003.

[27] L. A. Gallardo and M. A. Meju, "Joint two-dimensional cross-gradient imaging of magnetotelluric and seismic traveltime data for structural and lithological classification," *Geophys. J. Int.*, vol. 169, no. 3, pp. 1261–1272, 2007.

[28] J. Virieux and S. Operto, "An overview of full-waveform inversion in exploration geophysics," *Geophysics*, vol. 74, no. 6, pp. WCC1–WCC26, 2009.

[29] F. P. Mechel, *Formulas of Acoustics*. Berlin, Germany: Springer, 2008.

[30] W. C. Chew, *Waves and Fields in Inhomogeneous Media*. New York, NY, USA: Van Nostrand, 1995.

[31] K. A. Michalski and J. R. Mosig, "Multilayered media Green's functions in integral equation formulations," *IEEE Trans. Antennas Propag.*, vol. 45, no. 3, pp. 508–519, Mar. 1997.

[32] F. Li, Q. H. Liu, and L.-P. Song, "Three-dimensional reconstruction of objects buried in layered media using Born and distorted Born iterative methods," *IEEE Geosci. Remote Sens. Lett.*, vol. 1, no. 2, pp. 107–111, Apr. 2004.

[33] N. Linde, A. Tryggvason, J. E. Peterson, and S. S. Hubbard, "Joint inversion of crosshole radar and seismic traveltimes acquired at the South Oyster Bacterial Transport Site," *Geophysics*, vol. 73, no. 4, pp. G29–G37, 2008.

[34] A. Abubakar, M. Li, G. Pan, J. Liu, and T. M. Habashy, "Joint MT and CSEM data inversion using a multiplicative cost function approach," *Geophysics*, vol. 76, no. 3, pp. F203–F214, 2011.
[35] C. L. Lawson and R. J. Hanson, *Solving Least Squares Problems*, vol. 15. Philadelphia, PA, USA: SIAM, 1995.
[36] J. Shewchuk, "An introduction to the conjugate gradient method without the agonizing pain," Carnegie Mellon Univ., Pittsburgh, PA, USA, Tech. Rep. CMU-CS-94-125, Aug. 1994.

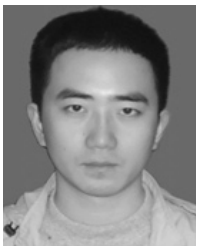

Tian Lan received the B.S. degree in electromagnetic fields and wireless technology and the M.S. degree in electromagnetic fields and microwave technology from the University of Electronic Science and Technology of China, Chengdu, China, in 2011 and 2014, respectively. He is currently pursuing the Ph.D. degree with Xiamen University, Xiamen, China.

His research interests include fast forward solvers in electromagnetics and acoustics, and joint inversion methods in multiphysical fields.

Hai Liu (S'11–M'13) received the B.E. and M.E. degrees in civil engineering from Tongji University, Shanghai, China, in 2007 and 2009, respectively, and the Ph.D. degree in environmental studies from Tohoku University, Sendai, Japan, in 2013.

He is currently an Assistant Professor with the Institute of Electromagnetics and Acoustics, Xiamen University, Xiamen, China. From 2013 to 2014, he was a Research Fellow with the Center for Northeast Asian Studies, Tohoku University. His research interests include the development of ground-penetrating radar systems and algorithms for a wide variety of applications, such as nondestructive testing in civil engineering, environmental monitoring, archeological investigation, and lunar exploration.

Na Liu received the Ph.D. degree in computational mathematics from the University of Chinese Academy of Sciences, Beijing, China, in 2013.

From 2012 to 2013, she was a Visiting Student with the Department of Electrical and Computer Engineering, Duke University, Durham, NC, USA. From 2013 to 2017, she held a post-doctoral position with Xiamen University, Xiamen, China, where she is currently an Associate Professor with the Institute of Electromagnetics and Acoustics. Her research interests include computational electromagnetics, especially the fast and efficient methods for complex media and their applications in cavities and optical waveguide problems.

Jinghe Li received the M.S. degree in geodetection and information technology from the Guilin University of Technology, Guilin, China, in 2009, and the Ph.D. degree in geophysics from the Institute of Geophysics and Geomatics, China University of Geosciences, Beijing, China, in 2015.

He is currently a Lecturer with the Guilin University of Technology. His research interests include seismic signal processing and forward and inversion in geophysics.

Feng Han received the B.S. degree in electronic science from Beijing Normal University, Beijing, China, in 2003, the M.S. degree in geophysics from Peking University, Beijing, in 2006, and the Ph.D. degree in electrical engineering from Duke University, Durham, NC, USA, in 2011.

He is currently an Assistant Professor with the Institute of Electromagnetics and Acoustics, Xiamen University, Xiamen, China. His research interests include ionosphere remote sensing by radio atmospherics, electromagnetic full-wave inversion by integral equations, reverse time migration image, and the design of an electromagnetic detection system.

Qing Huo Liu (S'88–M'89–SM'94–F'05) received the B.S. and M.S. degrees in physics from Xiamen University, Xiamen, China, in 1983 and 1986, respectively, and the Ph.D. degree in electrical engineering from the University of Illinois at Urbana–Champaign, Champaign, IL, USA, in 1989.

From 1986 to 1988, he was a Research Assistant with the Electromagnetics Laboratory, University of Illinois at Urbana–Champaign, where he was a Post-Doctoral Research Associate from 1989 to 1990. He was a Research Scientist and the Program Leader with Schlumberger-Doll Research, Ridgefield, CT, USA, from 1990 to 1995. From 1996 to 1999, he was an Associate Professor with New Mexico State University, Las Cruces, NM, USA. Since 1999, he has been with Duke University, Durham, NC, USA, where he is currently a Professor of electrical and computer engineering. He has authored over 400 papers in refereed journals and 500 papers in conference proceedings. His research interests include computational electromagnetics and acoustics, inverse problems, and their applications in nanophotonics, geophysics, biomedical imaging, and electronic packaging.

Dr. Liu is a fellow of the Acoustical Society of America, Electromagnetics Academy, and the Optical Society of America. He was a recipient of the 1996 Presidential Early Career Award for Scientists and Engineers from the White House, the 1996 Early Career Research Award from the Environmental Protection Agency, the 1997 CAREER Award from the National Science Foundation, and the 2017 ACES Technical Achievement Award. He also served as a Guest Editor of the PROCEEDINGS of the IEEE. Since 2015, he has been the Founding Editor-in-Chief of the new IEEE JOURNAL ON MULTISCALE AND MULTIPHYSICS COMPUTATIONAL TECHNIQUES. He served as an IEEE Antennas and Propagation Society Distinguished Lecturer from 2014 to 2016. Currently, he serves as the Deputy Editor-in-Chief of the *Progress in Electromagnetics Research*, an Associate Editor of the IEEE TRANSACTIONS ON GEOSCIENCE AND REMOTE SENSING, and an Editor of the *Journal of Computational Acoustics*.